MPM Spring Workshop - INRAE Aix-En-Provence
June 2, 2023

From multiphase formulations to earthquake triggered failures in MPM

Alba Yerro
ayerro@vt.edu

Assistant Professor
Department of Civil and Environmental Engineering, Virginia Tech

VIRGINIA TECH

Anura3D
MPM Research Community

Academic background

UNIVERSITAT POLITÈCNICA DE CATALUNYA
BARCELONATECH

UNIVERSITY OF CAMBRIDGE

VIRGINIA TECH

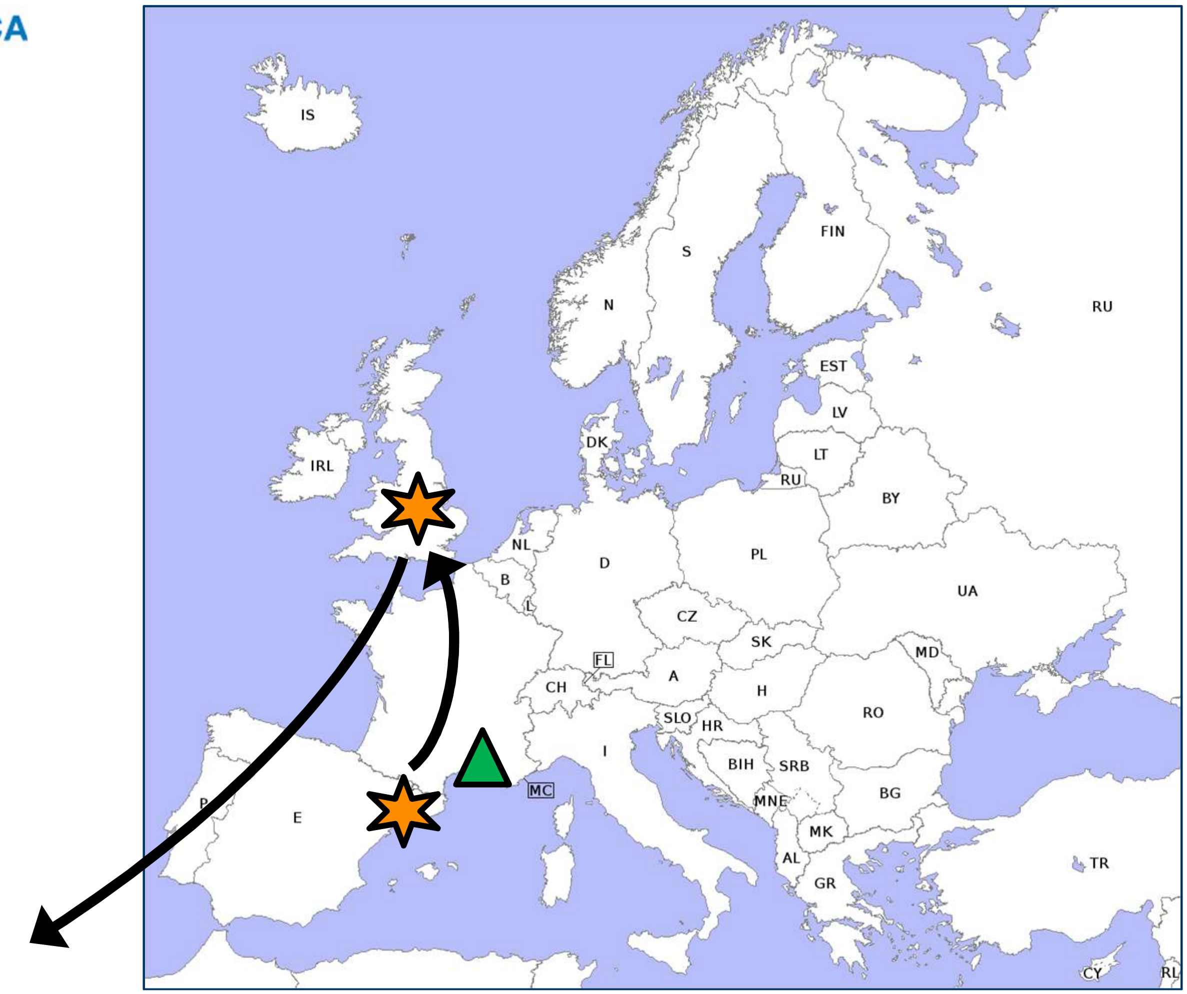

Motivation

Geotechnical problems ⟺ Soil-water-structure interactions & large deformations

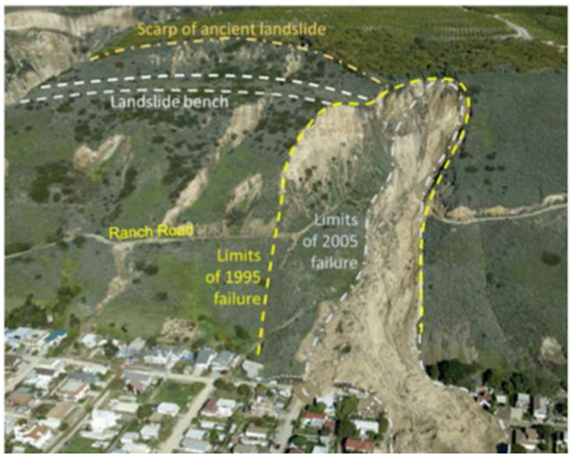

Conchita landslide, CA, 2005
(Geoengineer, 2020)

Edenville dam collapse, May 2020
(YouTube video by Lynn Coleman)

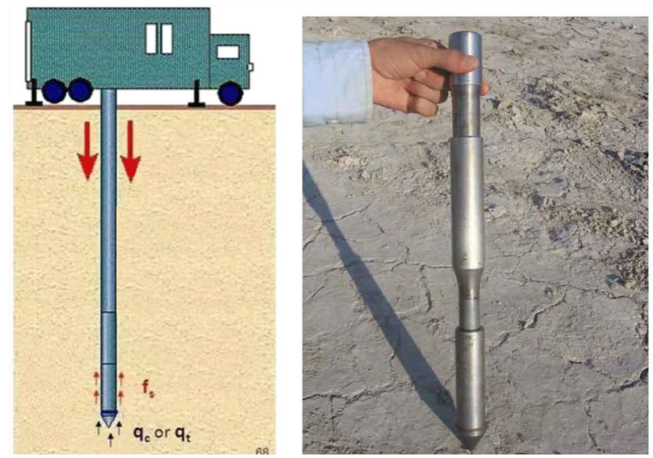

Cone penetration testing
(Firuze et al, 2019)

- Predicting consequences of geotechnical hazards is important for risk assessment.
- Studying large deformations, multi-phase, and multi-body interactions is challenging.
- Historically, geotechnical engineers focus on determining the stability of geotechnical systems.
- Classic techniques and state-of-practice numerical tools “only” estimate failure initiation.

Presentation outline

- Hydro-mechanical MPM formulations
  - Unsaturated framework
  - Internal erosion
- Earthquake triggered failures
  - Challenges in earthquake-triggered large-scale failures
  - Non-zero kinematic boundary conditions
  - Site response
    - Periodic boundary conditions
    - Generalized-α time integration scheme
  - Application

Rainfall and drawdown triggered slope failures

- Intense rainfall and rapid drawdown are leading causes of landslides and levee collapses around the world and have enormous social impacts every year.
- Climate change increases uncertainty.
- Complex boundaries including transient hydraulic head, seepage face, and infiltration/evaporation.
- Multi-phase formulations are needed to simulate saturated and unsaturated soils.

PETROPOLIS, Brazil, Feb 16, 2022
269 landslides recorded in the region
(Brazil's Civil Defense Secretariat)

Failure of the Wilnis levee in the Netherlands, August 26, 2003

MPM multi-phase formulations

- Dynamic coupled hydro-mechanical approaches capable of modelling large deformations in multi-phase conditions

Solid
Liquid
Gas

	1-phase (dry material)	2-phase (saturated)	2-phase + suction (unsaturated)	3-phase (unsaturated)
Single-layer approach	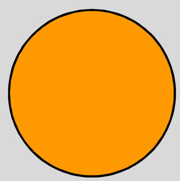	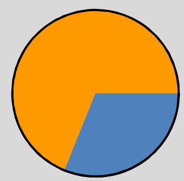	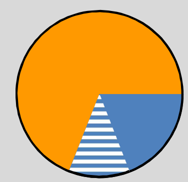 *Ceccato et al. (2021)*	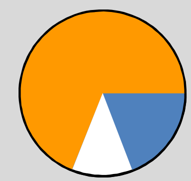 *Yerro et al. (2015)*
Multi-layer approach		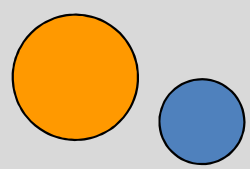	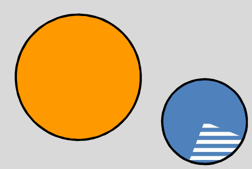	

3-Phase MPM formulation

Yerro et al (2015)

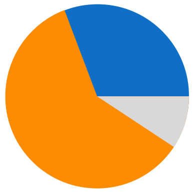

3-phase formulation

Yerro et al (2015,2016)

$\boldsymbol{a_s - a_l - a_g}$ **formulation** (fully dynamic)

General assumptions:

1. Solid grains are incompressible
2. Fluids are weakly compressible
3. Liquid flow follows Darcy's law
4. Isothermal conditions
5. No mass exchange between solid and fluid phases

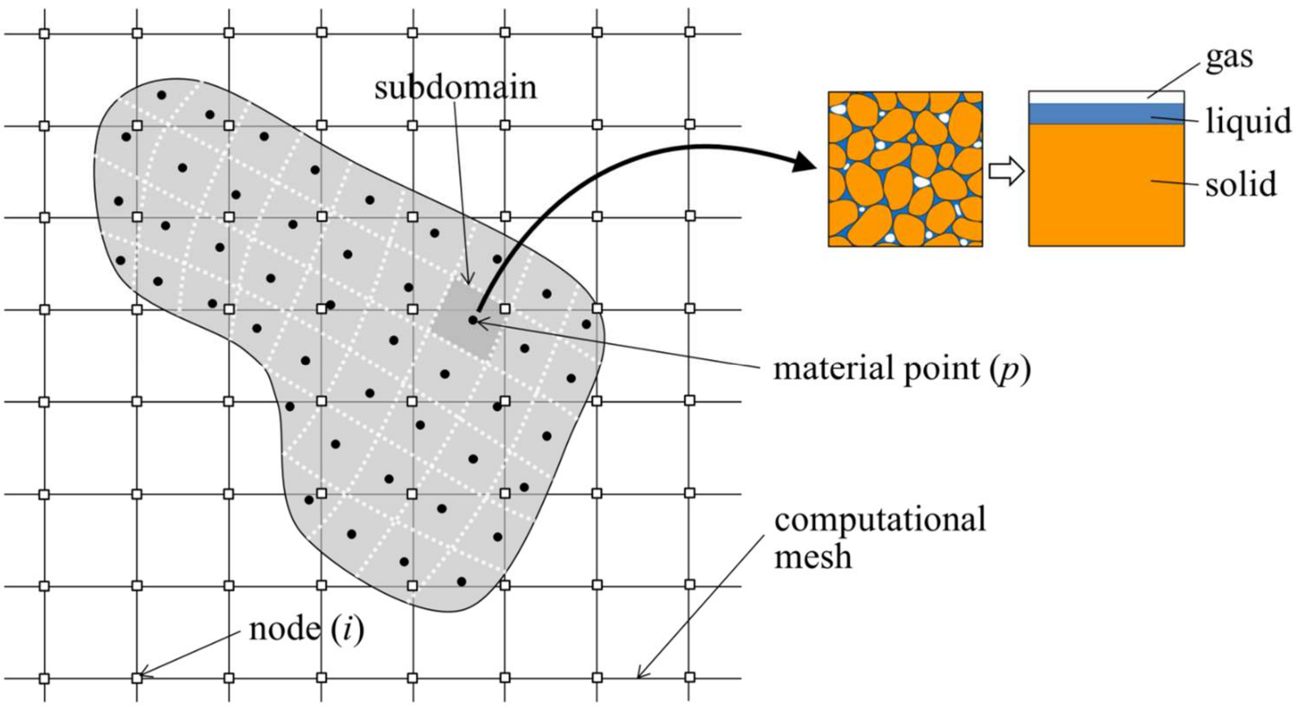

3-Phase MPM formulation

Yerro et al (2015)

1) Dynamic equilibrium Liquid

$$\rho_l \boldsymbol{a}_l = \nabla p_l - \boldsymbol{f}_l^d + \rho_l \mathbf{b}$$

2) Dynamic equilibrium Gas

$$\rho_g \boldsymbol{a}_g = \nabla p_g - \boldsymbol{f}_g^d + \rho_g \mathbf{b}$$

3) Dynamic equilibrium Mixture

$$\rho_s (1-n) \boldsymbol{a}_s + \rho_l n S_l \boldsymbol{a}_l + \rho_g n S_g \boldsymbol{a}_g = \nabla \cdot \boldsymbol{\sigma} + \rho_m \mathbf{b}$$

At the nodes

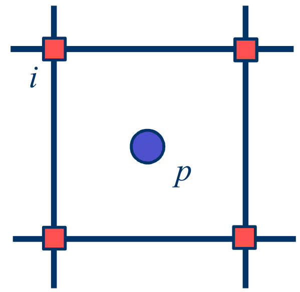

4) Mass balance Solid

$$\frac{Dn}{Dt} = (1-n) \nabla \cdot \boldsymbol{v}_S$$

5) Mass balance Liquid

$$n \frac{\partial(\rho_l S_l)}{\partial P_l} \dot{p}_l + n \frac{\partial(\rho_l S_l)}{\partial P_g} \dot{p}_g = \nabla \cdot [n S_l \rho_l (\mathbf{v}_l - \mathbf{v}_s)] - n S_l \rho_l \nabla \cdot \mathbf{v}_s$$

6) Mass balance Gas

$$n \frac{\partial(\rho_g S_g)}{\partial P_l} \dot{p}_l + n \frac{\partial(\rho_g S_g)}{\partial P_g} \dot{p}_g = \nabla \cdot [n S_g \rho_g (\mathbf{v}_g - \mathbf{v}_s)] - n S_g \rho_g \nabla \cdot \mathbf{v}_s$$

7) Constitutive equations

At the material points

Computational cycle

$t = t + \Delta t$

i

Initialization at a *mp* level

Nodal mass matrices, *nodal* forces, *nodal* velocities

Nodal non-advective fluxes $\mathbf{i}_l^a, \mathbf{i}_g^w$

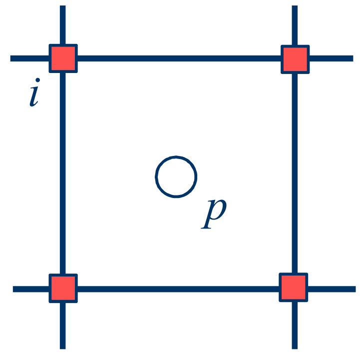

Dynamic Equilibrium Liquid

$$\tilde{\mathbf{M}}_\mathbf{l} \cdot \dot{\mathbf{v}}_\mathbf{l} = \mathbf{F}_\mathbf{l}^{\mathbf{ext}} - \mathbf{F}_\mathbf{l}^{\mathbf{int}} - \mathbf{Q}_\mathbf{l} \cdot \left(\mathbf{v}_\mathbf{l} - \mathbf{v}_\mathbf{s}\right)$$

Dynamic Equilibrium Gas

$$\tilde{\mathbf{M}}_\mathbf{g} \cdot \dot{\mathbf{v}}_\mathbf{g} = \mathbf{F}_\mathbf{g}^{\mathbf{ext}} - \mathbf{F}_\mathbf{g}^{\mathbf{int}} - \mathbf{Q}_\mathbf{g} \cdot \left(\mathbf{v}_\mathbf{g} - \mathbf{v}_\mathbf{s}\right)$$

Dynamic Equilibrium Mixture

$$\mathbf{M}_\mathbf{s} \cdot \dot{\mathbf{v}}_\mathbf{s} + \mathbf{M}_\mathbf{l} \cdot \dot{\mathbf{v}}_\mathbf{l} + \mathbf{M}_\mathbf{g} \cdot \dot{\mathbf{v}}_\mathbf{g} = \mathbf{F}^{\mathbf{ext}} - \mathbf{F}^{\mathbf{int}}$$

Updating *nodal* velocities

Updating *mp* velocities

Updating *mp* strains

Mass balance water

$$n\frac{\partial \xi^w}{\partial p_l}\dot{p}_l + n\frac{\partial \xi^w}{\partial p_g}\dot{p}_g = -\nabla\cdot\left[n\xi_g^w\left(\mathbf{v}_g - \mathbf{v}_s\right)\right] - \nabla\cdot\left[n\xi_l^w\left(\mathbf{v}_l - \mathbf{v}_s\right)\right] - \xi^w\nabla\cdot\mathbf{v}_s - \nabla\cdot\mathbf{i}_g^w$$

Mass balance air

$$n\frac{\partial \xi^a}{\partial p_l}\dot{p}_l + n\frac{\partial \xi^a}{\partial p_g}\dot{p}_g = -\nabla\cdot\left[n\xi_g^a\left(\mathbf{v}_g - \mathbf{v}_s\right)\right] - \nabla\cdot\left[n\xi_l^a\left(\mathbf{v}_l - \mathbf{v}_s\right)\right] - \xi^a\nabla\cdot\mathbf{v}_s - \nabla\cdot\mathbf{i}_l^a$$

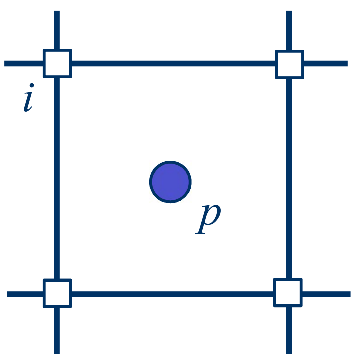

Constitutive equation

$$\dot{\boldsymbol{\sigma}}' = \mathbf{D} : \dot{\boldsymbol{\varepsilon}} + \mathbf{h}'\dot{s}$$

Hydraulic constitutive equations

Updating stresses and other *mp* properties

p

Rainfall triggered slope failures

Yerro et al (2015)

Girona road embankments, 2010

- Embankments were subjected to heavy rainfall
- Shallow failures were observed
- The slides moved downwards 2-4 m

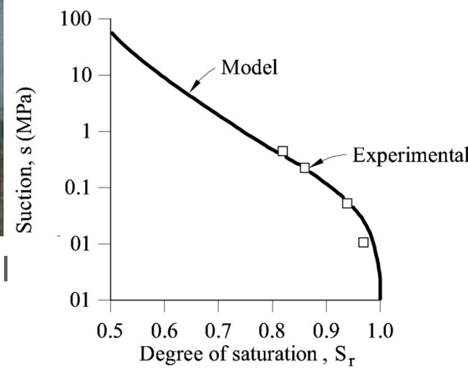

s= 800 kPa → 0kPa

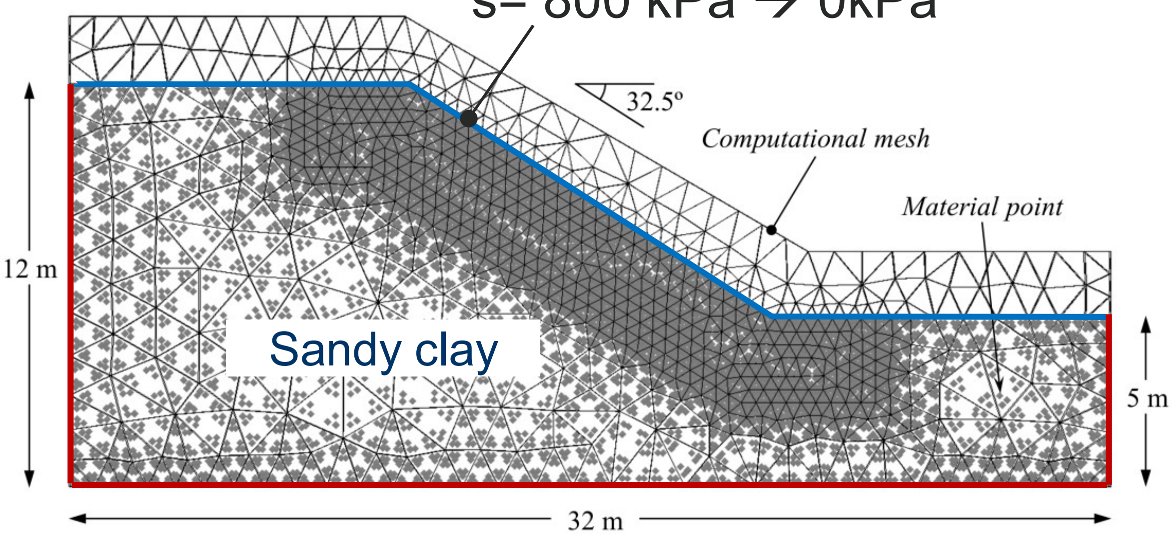

Numerical parameters

Number of elements	3654	
Number of material points	7593	
Damping factor α	0.05	
Time step	$2\cdot10^{-4}$	s

General characteristics of the soil

Solid density	2700	kg/m^3
Porosity	0.35	
Poisson's coefficient	0.33	
Liquid density	1000	kg/m^3
Gas density	1	kg/m^3
Liquid bulk modulus	100	MPa
Gas bulk modulus	0.01	MPa
Liquid viscosity	10^{-3}	kg/m·s
Gas viscosity	10^{-6}	kg/m·s
Intrinsic permeability liquid	10^{-10}	m^2
Intrinsic permeability gas	10^{-11}	m^2

M-C suction-dependence param.

Young's modulus	10	MPa
Cohesion c'	1	kPa
Friction angle φ'	20	º
Δc_{max}	15	kPa
B	0.07	
A	0.01	

Suction-dependent Mohr-Coulomb model

Yerro et al (2015)

Yield function

$$q = c\cos\varphi + \bar{p}\sin\varphi$$

Softening rules (wetting softening)

$$\begin{cases} c = c' + \Delta c_{max}\left(1 - e^{-B(s/p_{atm})}\right) \\ \varphi = \varphi' + A\dfrac{s}{p_{atm}} \end{cases}$$

s suction

$\bar{\sigma}$ constitutive stress (net stress)

c, φ cohesion, friction angle

c', φ' cohesion, friction angle (sat cond.)

p_{atm} atmospheric pressure (100 kPa)

$A, B, \Delta c_{max}$ calibration parameters

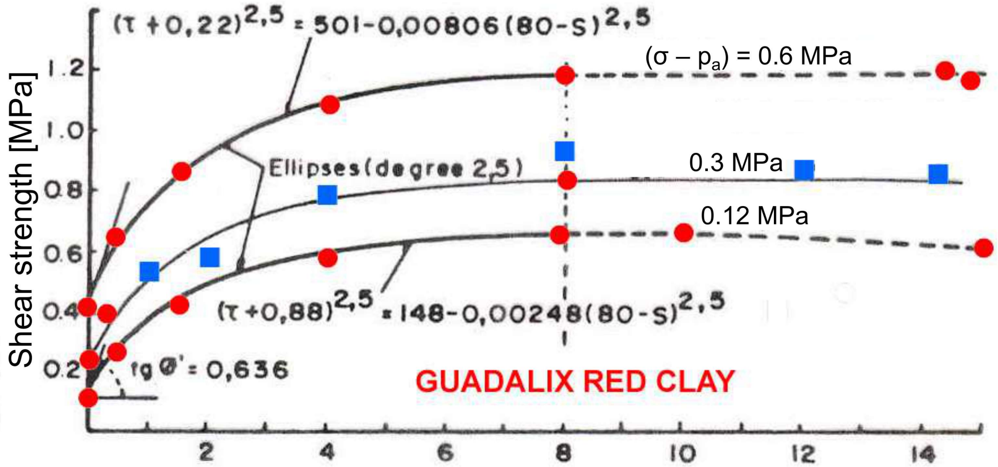

Suction ($p_a - p_g$) [MPa]

Variation of shear strength with suction and vertical stress. Guadalix red clay *(Escario & Jucá, 1989)*

Rainfall triggered slope failures

Yerro et al (2015)

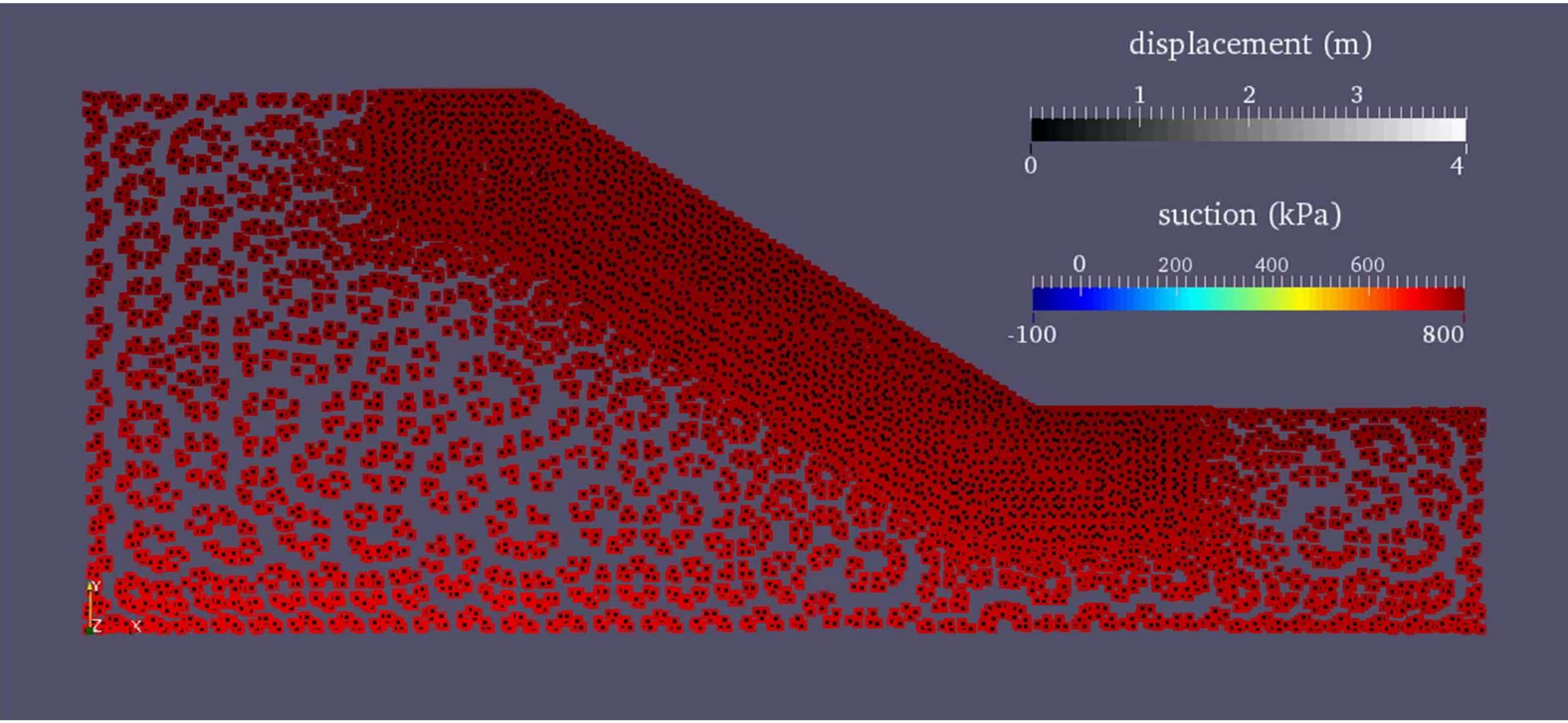

MPM approaches for unsaturated soils

Yerro et al. (2022)

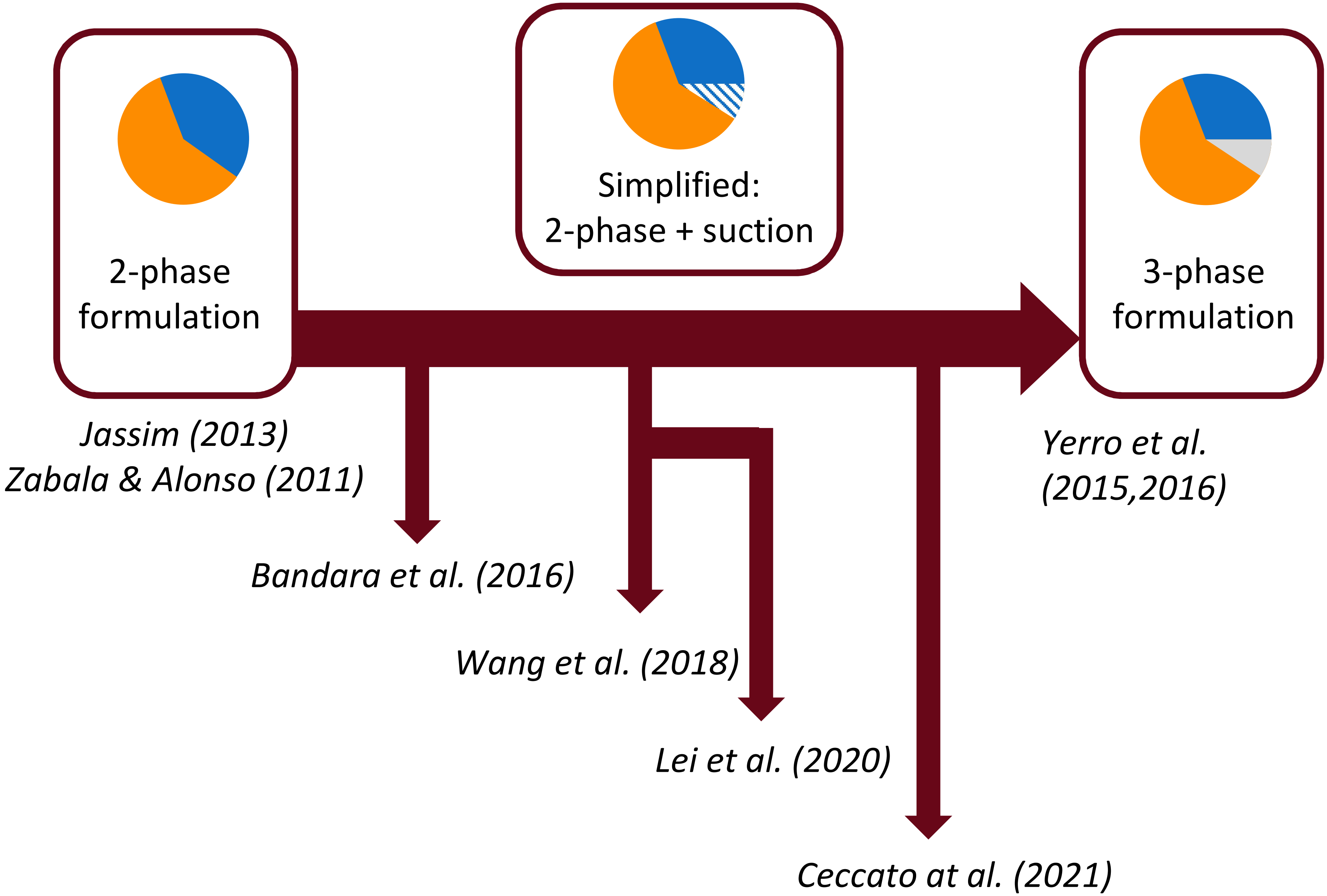

2-Phase + suction MPM formulation

Ceccato et al. (2021)
Yerro et al. (2022)

1) Dynamic equilibrium Liquid

$$\rho_l \boldsymbol{a}_l = \nabla p_l - \boldsymbol{f}_l^d + \rho_l \mathbf{b}$$

2) Dynamic equilibrium Gas

$$\cancel{\rho_g \boldsymbol{a}_g = \nabla p_g - \boldsymbol{f}_g^d + \rho_g \mathbf{b}}$$

3) Dynamic equilibrium Mixture

$$\rho_s(1-n)\boldsymbol{a}_s \ldots$$

4) Mass balance

$$\frac{Dn}{Dt} = (1-n \ldots$$

flux due to spatial variations of fluid masses

$$nS_l\rho_l \nabla \cdot (\mathbf{v}_l - \mathbf{v}_s) + \boxed{(\mathbf{v}_l - \mathbf{v}_s) \cdot \nabla (nS_l\rho_l)}$$

5) Mass balance Liquid

$$n\frac{\partial(\rho_l S_l)}{\partial P_l}\dot{p}_l + \cancel{n\frac{\partial(\rho_l S_l)}{\partial P_g}\dot{p}_g} = \nabla \cdot [nS_l\rho_l(\mathbf{v}_l - \mathbf{v}_s)] - nS_l\rho_l \nabla \cdot \mathbf{v}_s$$

6) Mass balance Gas

$$\cancel{n\frac{\partial(\rho_g S_g)}{\partial P_l}\dot{p}_l + n\frac{\partial(\rho_g S_g)}{\partial P_g}\dot{p}_g = \nabla \cdot [nS_g\rho_g(\mathbf{v}_g - \mathbf{v}_s)] - nS_g\rho_g \nabla \cdot \mathbf{v}_s}$$

7) Constitutive equations

At the nodes

At the material points

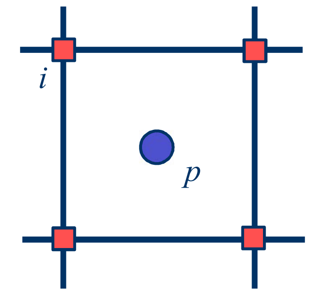

2-Phase + suction MPM formulation

Yerro et al (2015)

- Effect of including all terms from advective fluxes in 1D infiltration problem

Linear SWRC $S_L = 1 - a_v(p_G - p_L)$

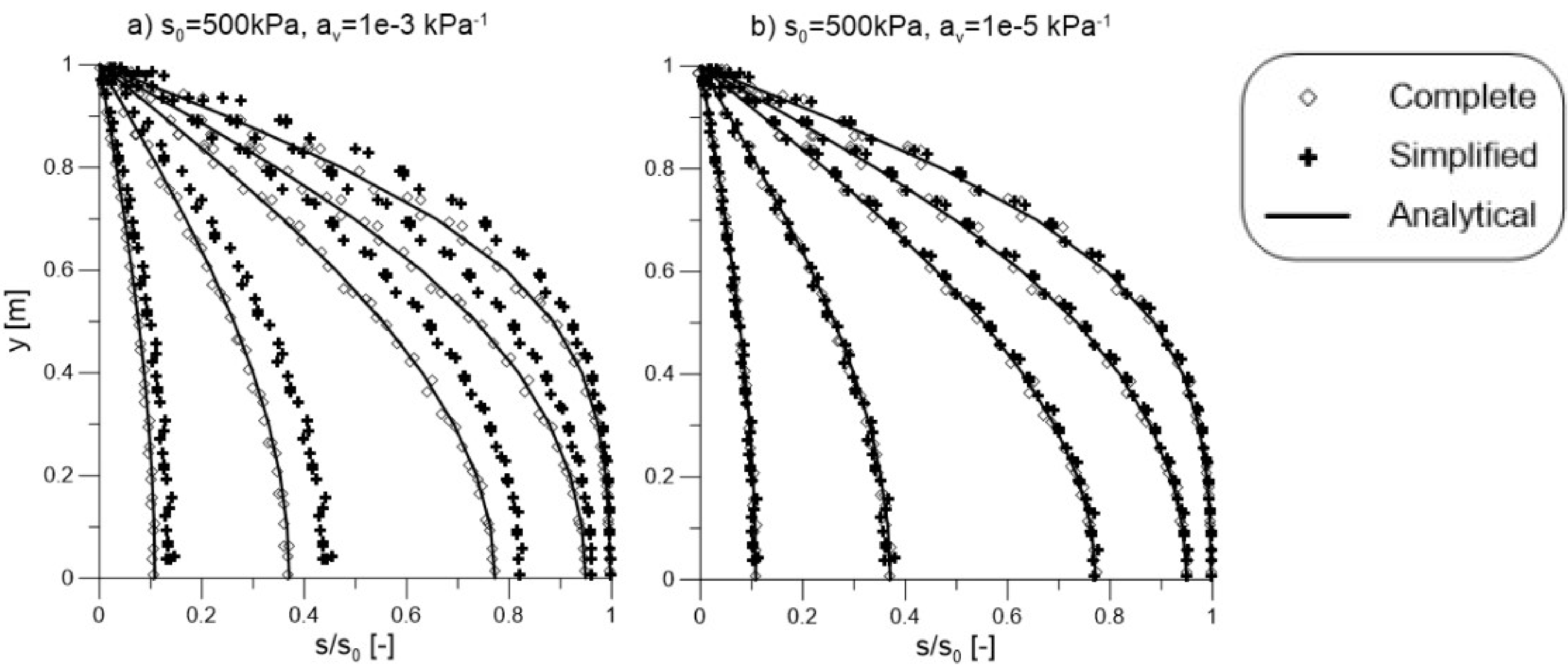

Rainfall and drawdown triggered slope failures

PhD student
Veronica Girardi

- Drawdown in River side

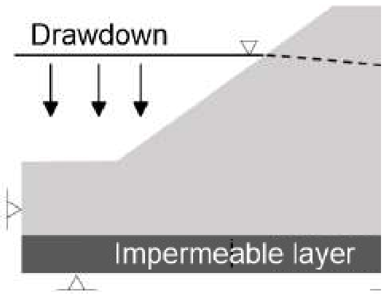

- Rainfall in Land side

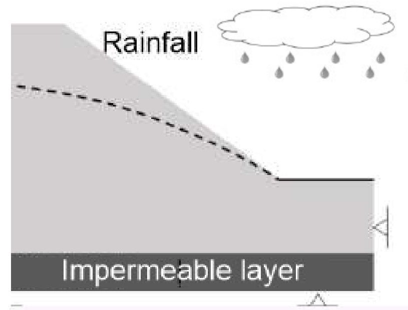

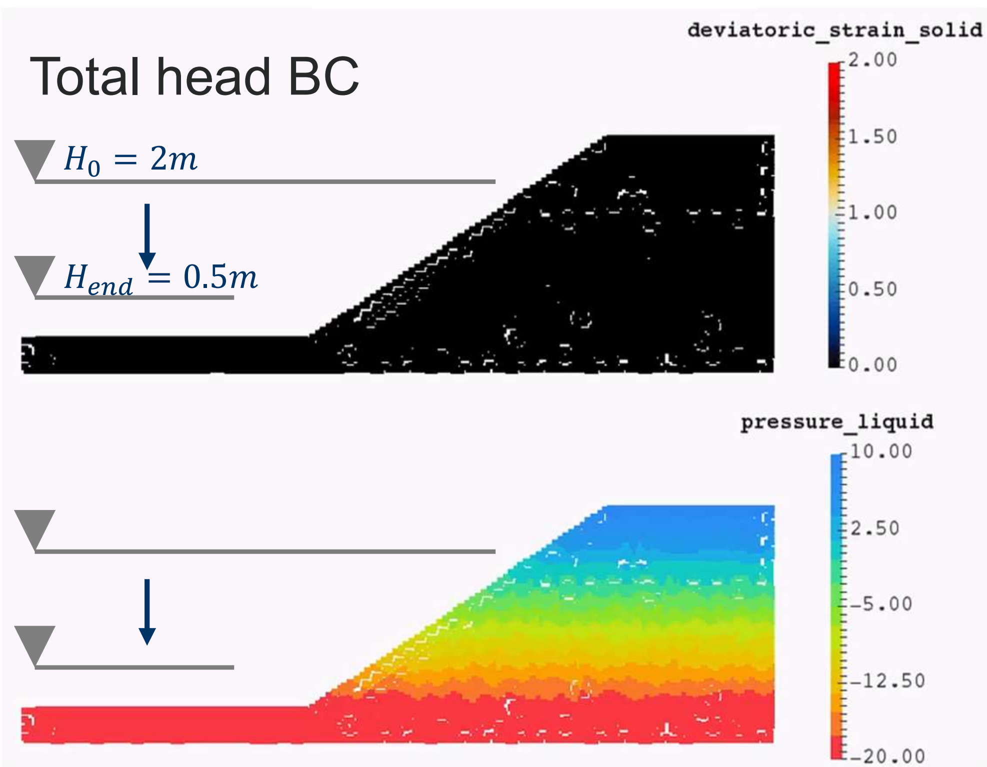

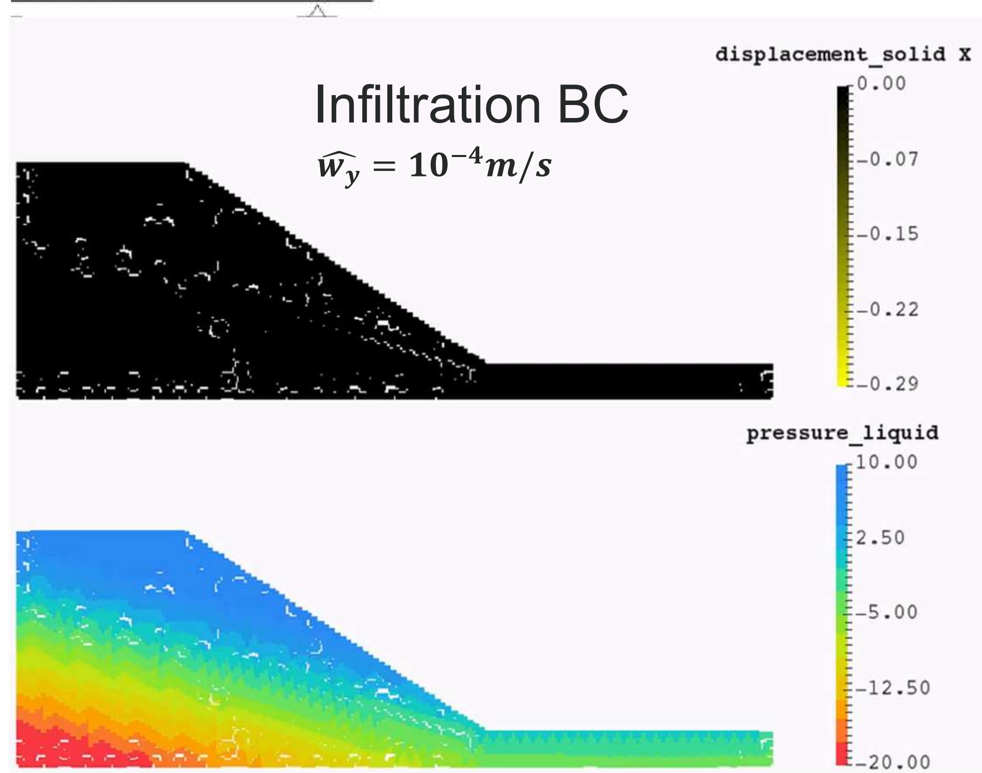

Girardi et al. (2021)

Internal Erosion

Teton Dam Failure

- Internal erosion is the mobilization of particles in a soil mass as a result of seepage
- Critical geotechnical hazard
- One of the leading causes of failures in levees and earth dams
- “Small-scale” mechanism that has “large-scale” consequences

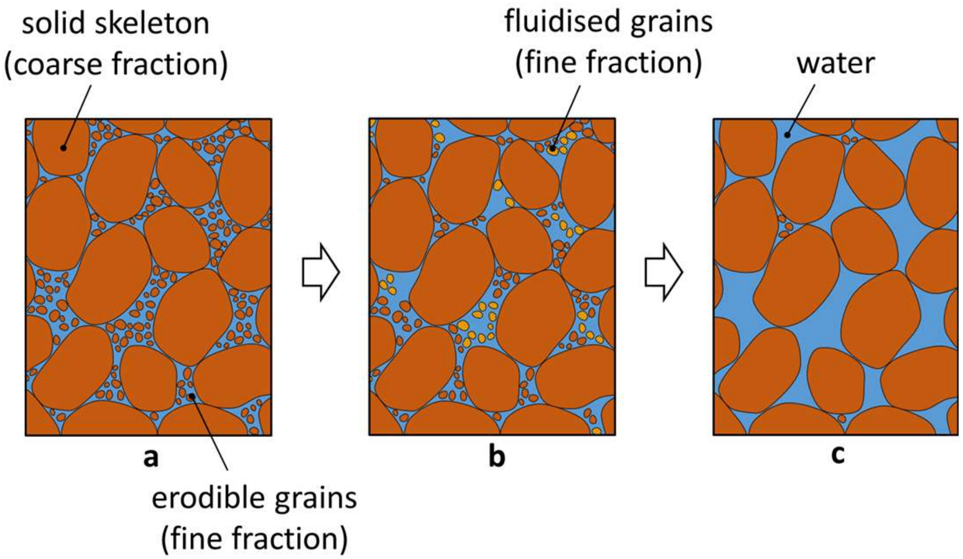

Mass transfer from solid to liquied phases

MPM multi-phase formulations

- Dynamic coupled hydro-mechanical approaches capable of modelling large deformations in multi-phase conditions

Solid
Liquid
Gas

	1-phase (dry material)	2-phase (saturated)	2-phase + suction (unsaturated)	3-phase (unsaturated)
Single-layer approach	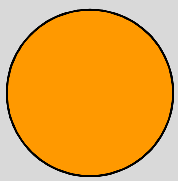	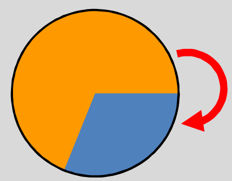 *Yerro et al. (2017)*	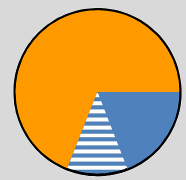	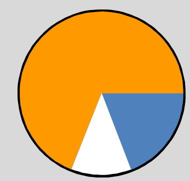
Multi-layer approach		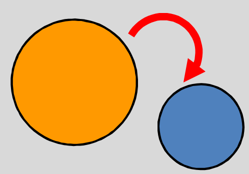 *Murphy et al. (2021)*	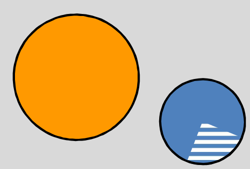	

Presentation outline

- Hydro-mechanical MPM formulations
  - Unsaturated framework
  - Internal erosion
- Earthquake triggered failures
  - Challenges in earthquake-triggered large-scale failures
  - Non-zero kinematic boundary conditions
  - Site response
    - Periodic boundary conditions
    - Generalized-α time integration scheme
  - Application

Earthquake-triggered failures

- Large slope deformation occurs in approximately 46% of earthquake events (Bird and Bommer, 2004).
- Current predictive methods (e.g., Newmark methods) cannot capture large runouts and complex non-linear soil behavior (e.g., liquefaction).
- Fundamental questions regarding mechanics of triggering and post-failure mobility.

*Mejia embankment,
2016 Mw 7.8 Pedernales,
Ecuador*

*Vine road embankment,
2018 Mw 7.0 Anchorage, Alaska*

*Coastal landslide,
2017 Mw 3.5 Big Sur,
California*

Challenges in earthquake-triggered large-scale failures

- Complex geometry and stratigraphy
- Site response (amplification/attenuation of seismic waves)
- Treatment of boundary conditions
- Constitutive models (cyclic loading – kinematic hardening)

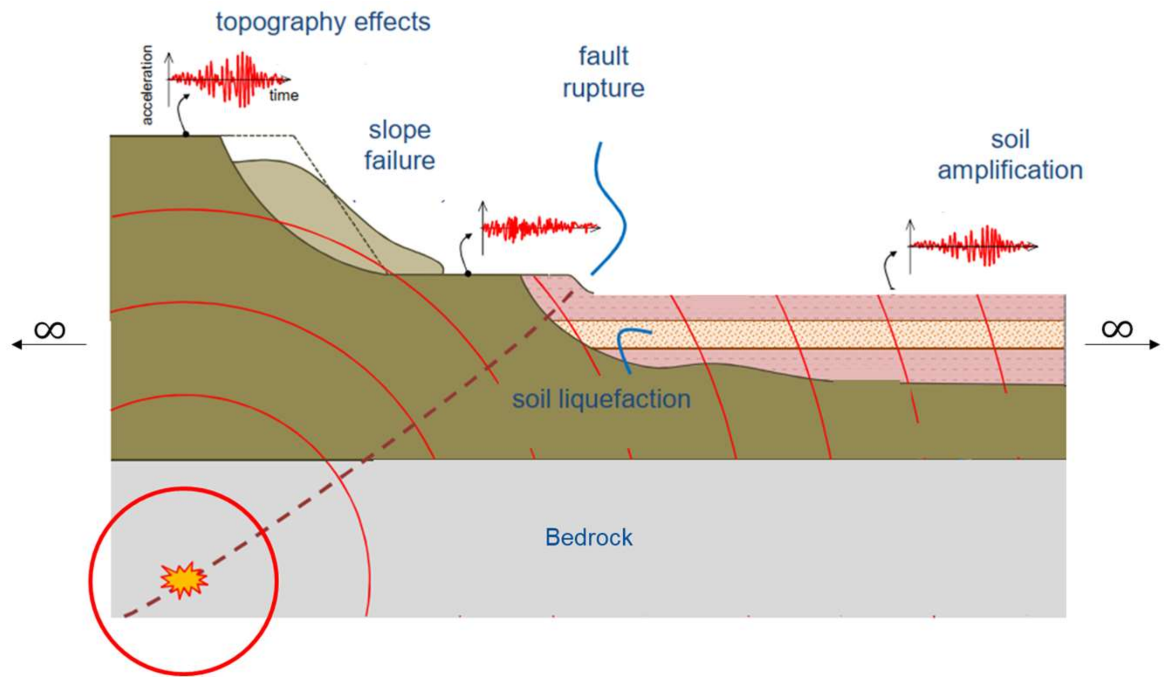

Earthquake-triggered failures

PhD student:
Abdel Alsardi

Non-zero kinematic boundary condition

- Prescribe motion at the boundary nodes (time-dependent Dirichlet boundary condition)
- Moving mesh

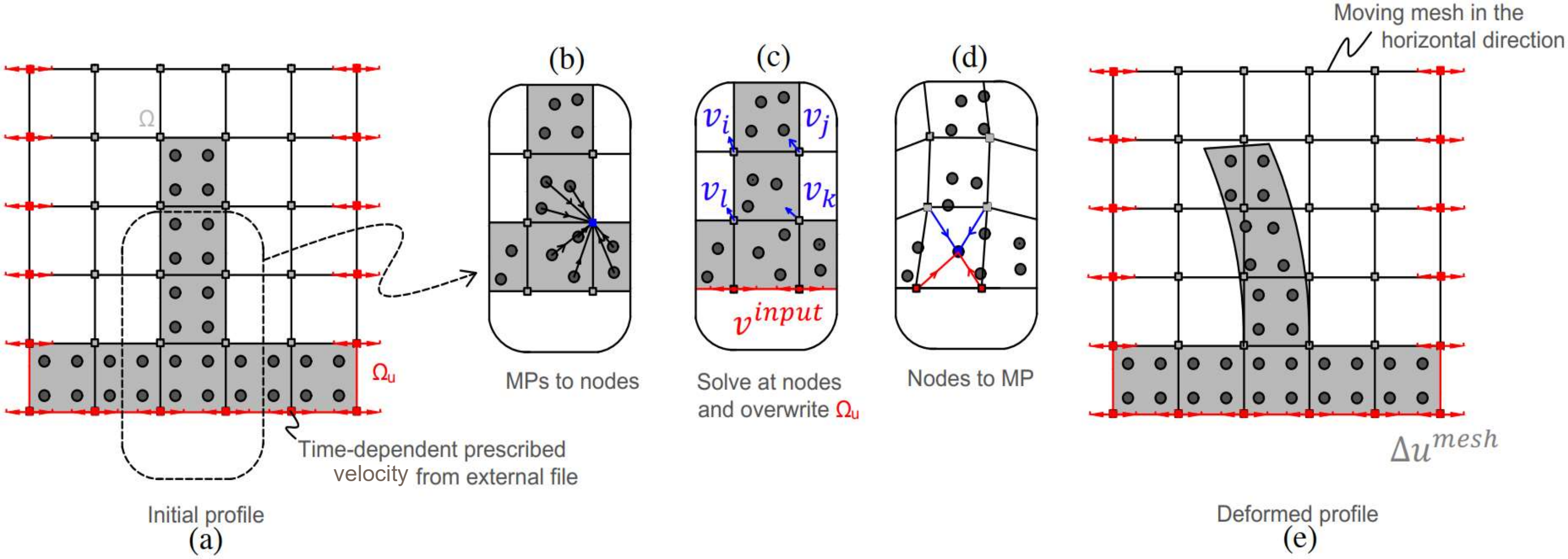

Alsardi et al. (2021)

Small-scale shaking table experiment

Alsardi et al. (2021)

Experimental model (Wartman, 1999)

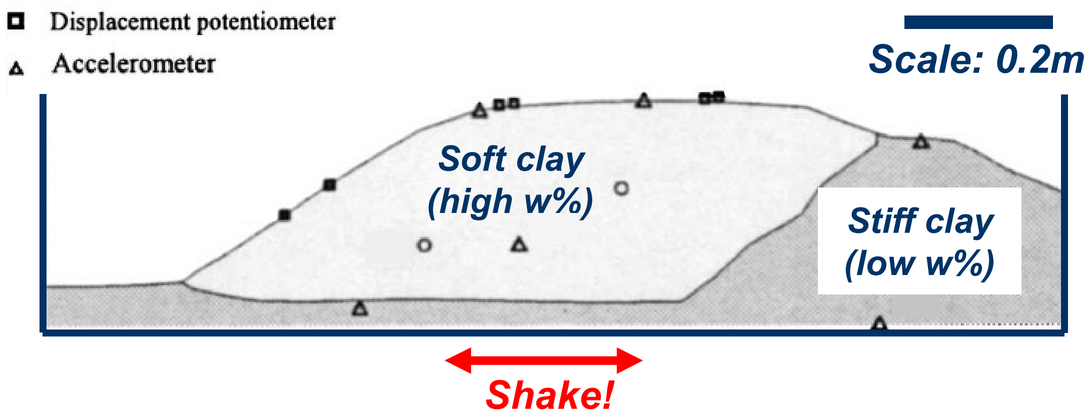

- Small-scale slope testing program on synthetic clay
- Clay presented strain-softening behavior

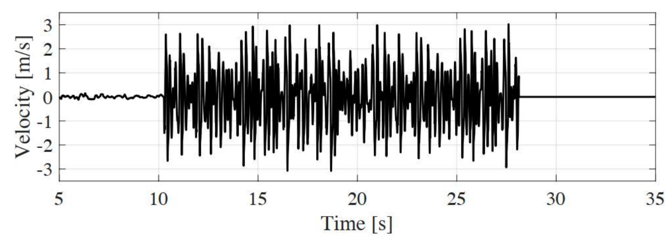

MPM model

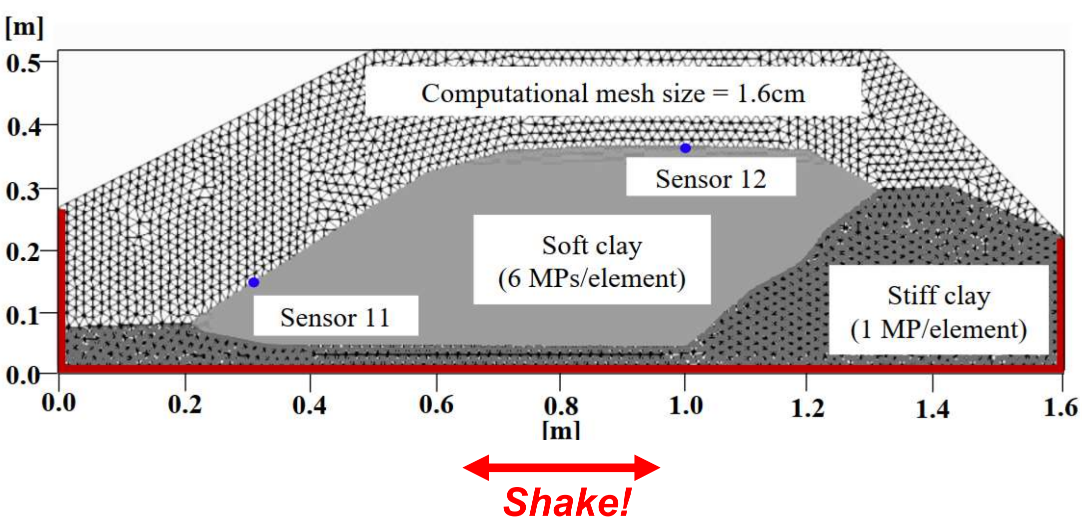

- Stress-strain calibration with lab data
- Strain-rate effects and shear modulus degradation are not incorporated

Parameter	Soft Clay	Stiff Clay
Saturated unit weight, γ [kN/m^3]	13.6	13.6
Peak undrained strength, $S_{u,peak}$ [kPa]	2.68	5.90
Residual undrained strength, $S_{u,resd}$ [kPa]	1.77	4.03
Undrained poisson ratio, ν_u [-]	0.485	0.485
Undrained small-strain stiffness, E_u [kPa]	615	4190

Small-scale shaking table experiment

Alsardi et al. (2021)

MPM results and validation

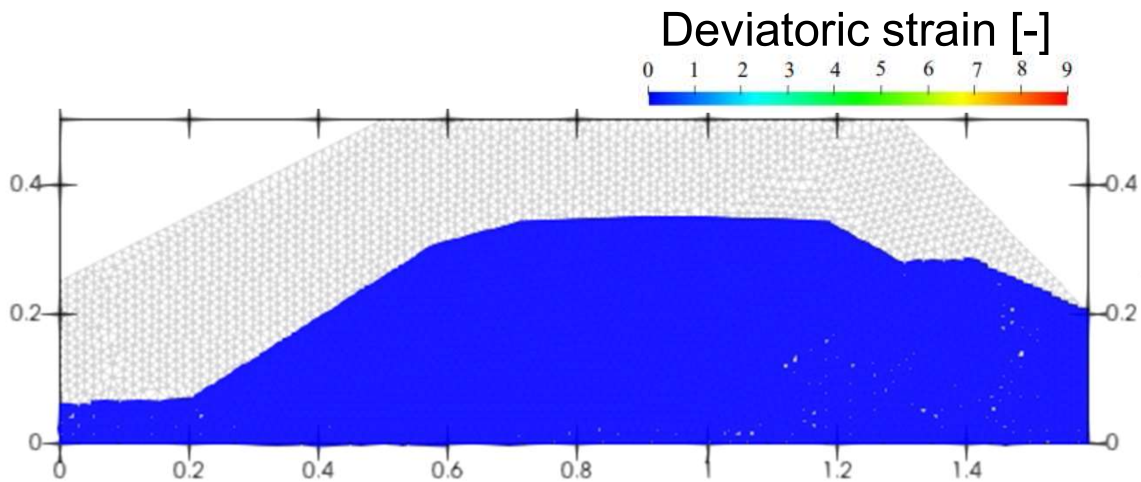

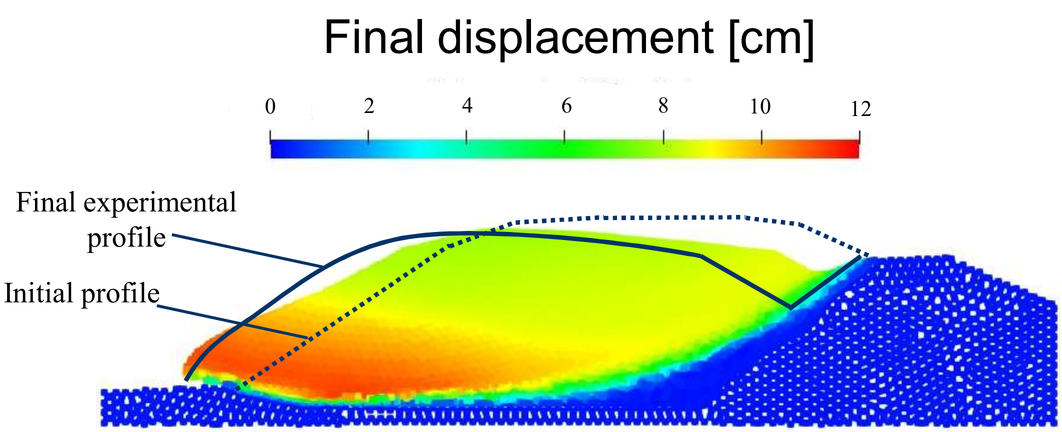

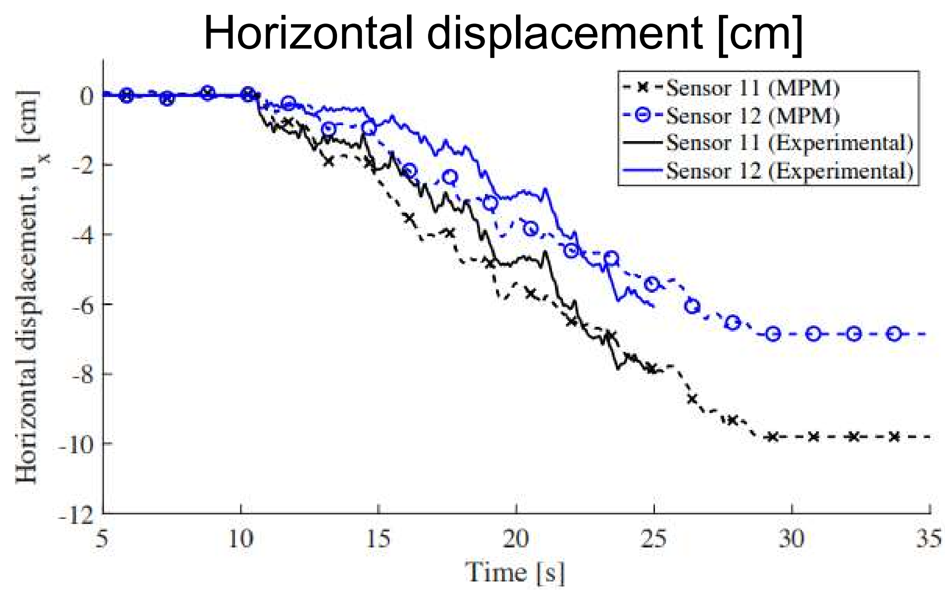

Earthquake-triggered failures

Alsardi & Yerro (2023)

Site response analysis

- Simulation of a fee-field column

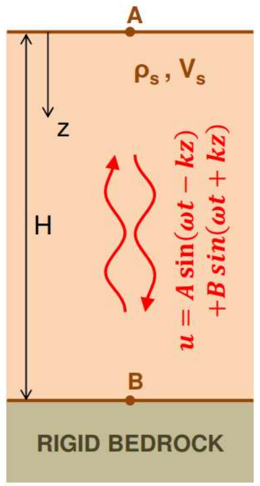

- Implementation of Periodic Boundary Conditions
  - Ensure identical displacement for the nodes at the same spatial level.
  - Implementation: overwriting the degrees of freedom to ensure the same nodal solution, sharing information between node sets.
  - MP relocation technique.

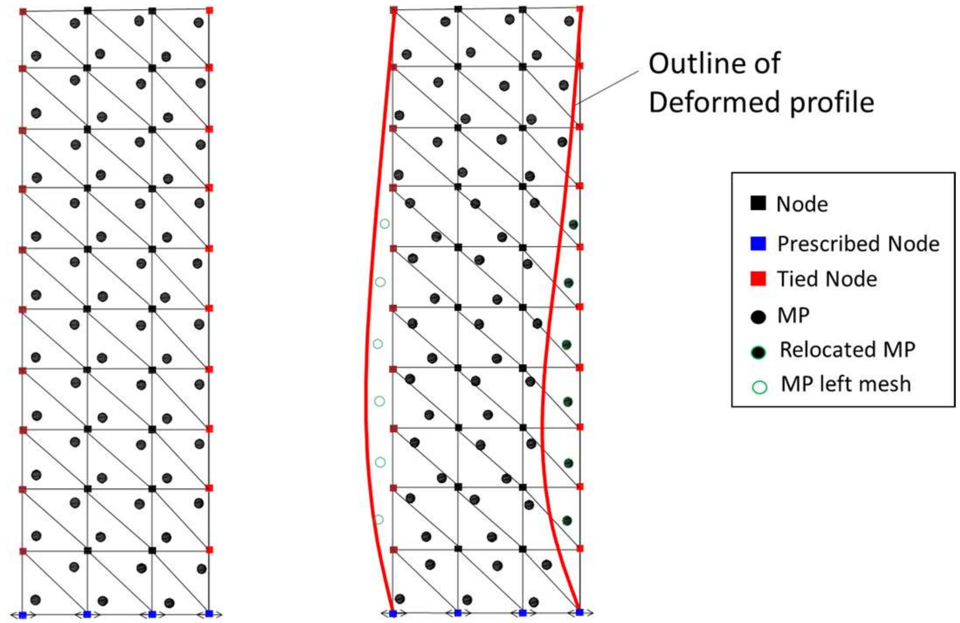

(a) Initial profile (b) Deformed profile

Time integration scheme

- Traditionally MPM uses explicit Euler-Cromer scheme.
- Euler-Cromer induces spurious high-frequency noise.
- Reduces the accuracy of numerically predicted site response.

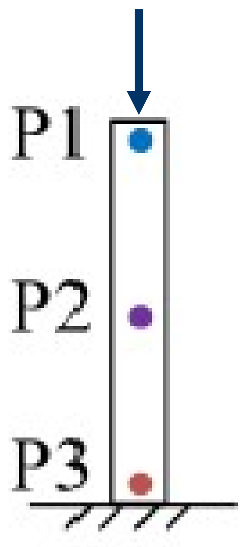

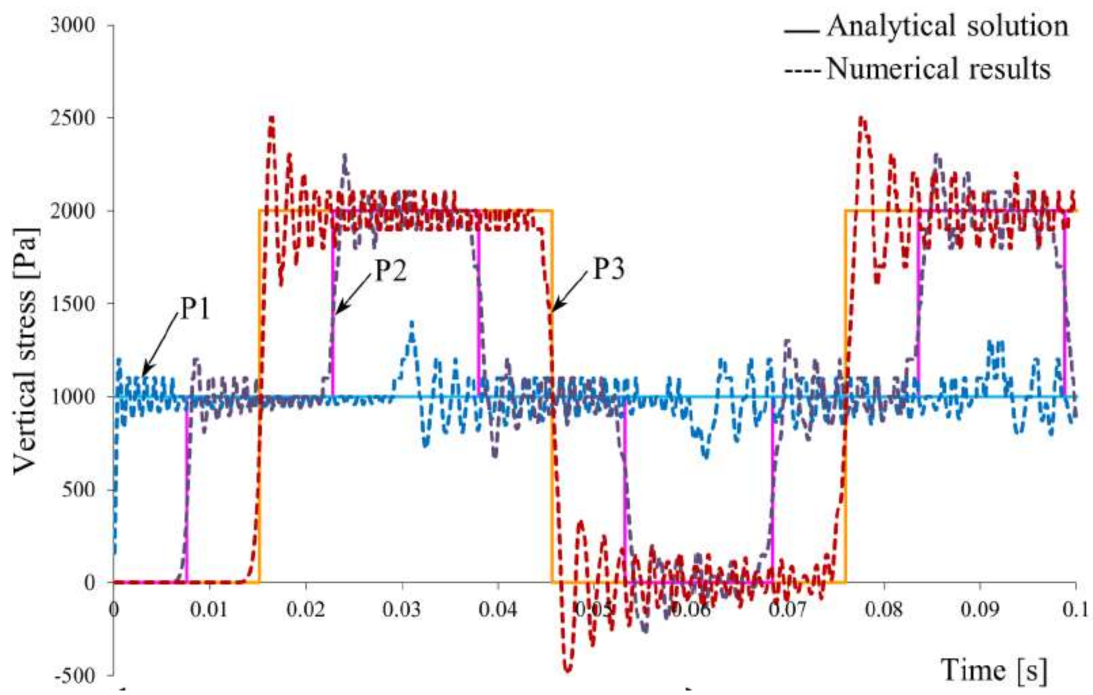

Explicit Generalized-α scheme

- A more general implementation of the Newmark-type family.
- User-controlled dissipation of higher frequencies.

- Time scheme characteristics:
  - Maximum dissipation of high-frequency noise.
  - Minimal dissipation of low-frequency modes.
  - Second-order accuracy.

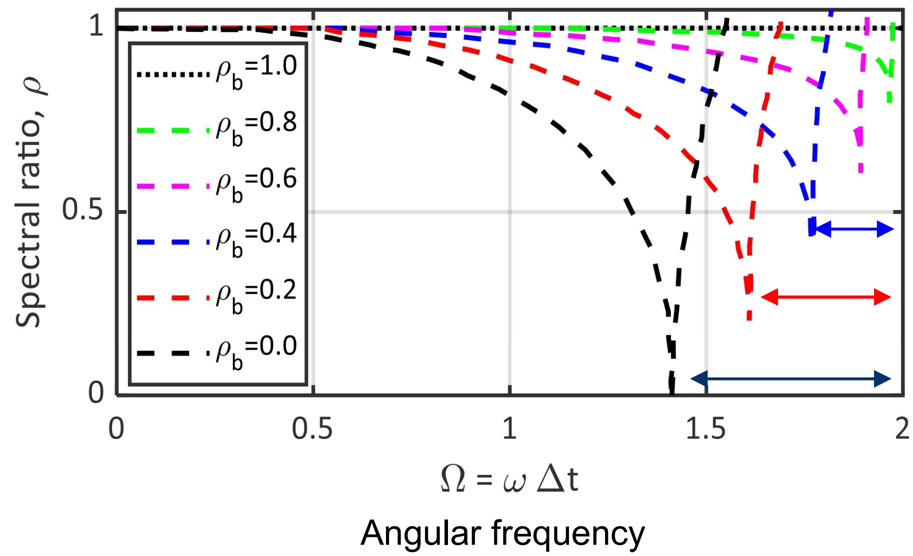

- Implementation:
  - Explicit scheme based on Hulbert and Chung (1996).
  - Evaluate acceleration at an intermediate step.

- Stability:
  - Depends on the selection of minimal spectral ratio, ρ_b, and time step, Δt.
  - Courant-Frederichs-Levy condition

Explicit Generalized-α scheme

1. Compute initial nodal mass and nodal forces: M_i^t , $\vec{f}_i^{ext,t}$, $\vec{f}_i^{int,t}$

2. Compute intermediate nodal acceleration at $t + \Delta t\ (1 - \alpha_m)$: $\vec{a}_i^{t+\Delta t\ (1-\alpha_m)} = \dfrac{\vec{f}_i^t}{M_i^t}$

3. Compute final nodal acceleration at $t + \Delta t$: $\vec{a}_i^{t+\Delta t} = \dfrac{\vec{a}_i^{t+\Delta t(1-\alpha_m)} - \alpha_m\, \vec{a}_i^t}{1 - \alpha_m}$

4. Compute MP velocity at $t + \Delta t$: $\vec{v}_{MP}^{t+\Delta} = \vec{v}_{MP}^t + \Sigma_{i=1}^{n_{el}} \vec{N}_i \left[(1-\gamma)\vec{a}_i^t + \gamma\, \vec{a}_i^{t+\Delta t}\right]\Delta t$

5. Compute nodal velocity at $t + \Delta t$: $\vec{v}_i^{t+\Delta t} = \dfrac{\Sigma_{n_{el}}\Sigma_{n_{MP}}\, m_{MP}\, \vec{v}_{MP}^{t+\Delta t}}{M_i^t}$

6. Compute displacements at $t + \Delta t$:

$$\vec{u}_{MP}^{t+\Delta t} = \vec{u}_{MP}^t + \vec{v}_{MP}^{t+\Delta t}\Delta t + \Sigma_{i=1}^{n_{el}} \vec{N}_i \left[\left(\frac{1}{2} - \beta_m\right)\vec{a}_i^t + \beta_m \vec{a}_i^{t+\Delta t}\right](\Delta t)^2$$

Alsardi & Yerro (2023)

Verification model

- Comparison with:
  1. PLAXIS (FEM, Newmark-β)
  2. Linear solution

- Assuming linear elastic material.

Parameter	Value
Constitutive model	Linear-elastic
Young's modulus, E (kPa)	10^4, $1.85\text{x}10^5$, $10\text{x}10^5$
Poisson ratio, ν (-)	0.33

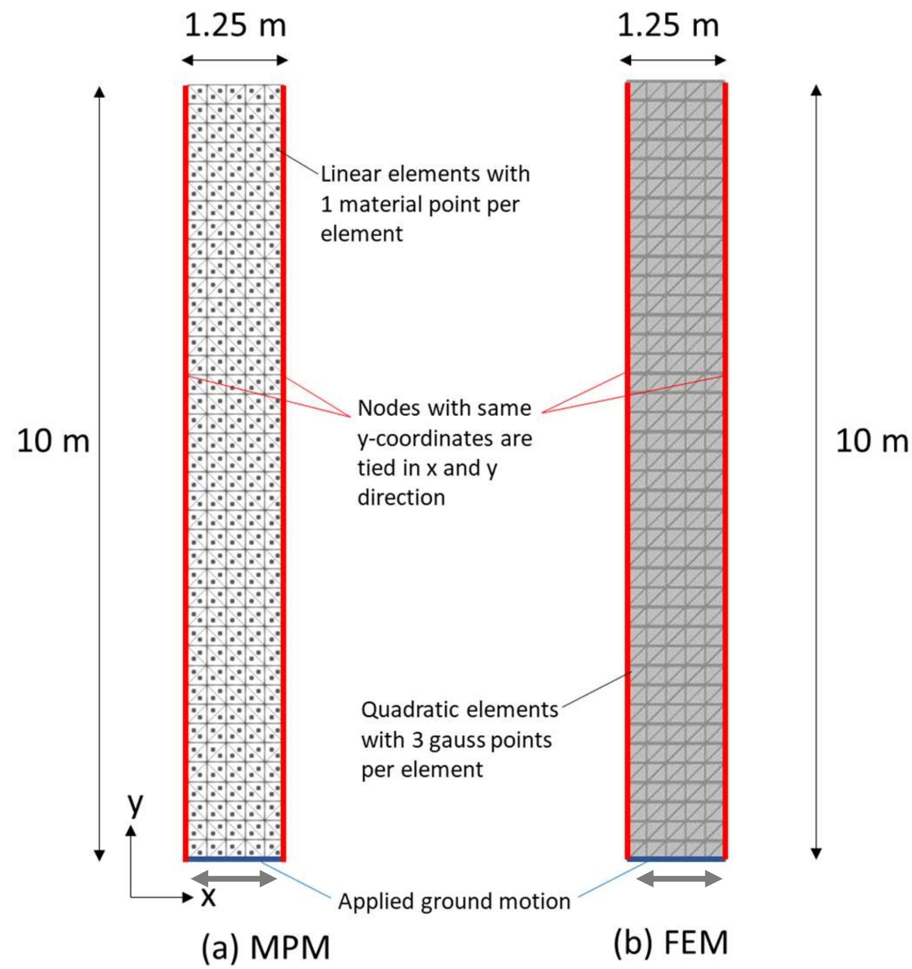

Alsardi, A. and Yerro, A. (2022) Coseismic site response and slope instabilities using periodic boundary conditions in MPM. Journal of Rock Mechanics and Geotechnical Engineering – accepted

Small deformation - irregular cyclic loading

Alsardi & Yerro (2023)

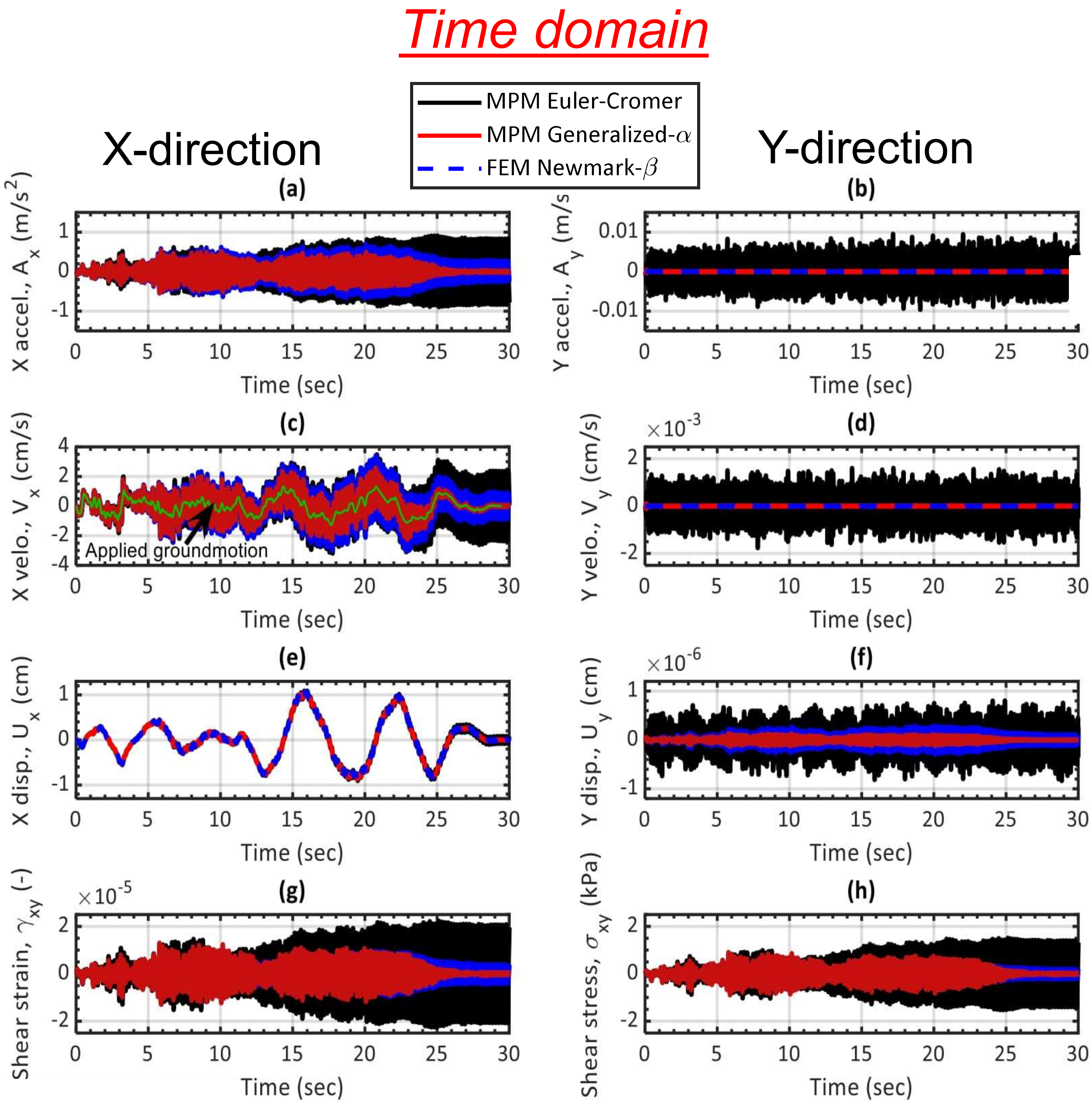

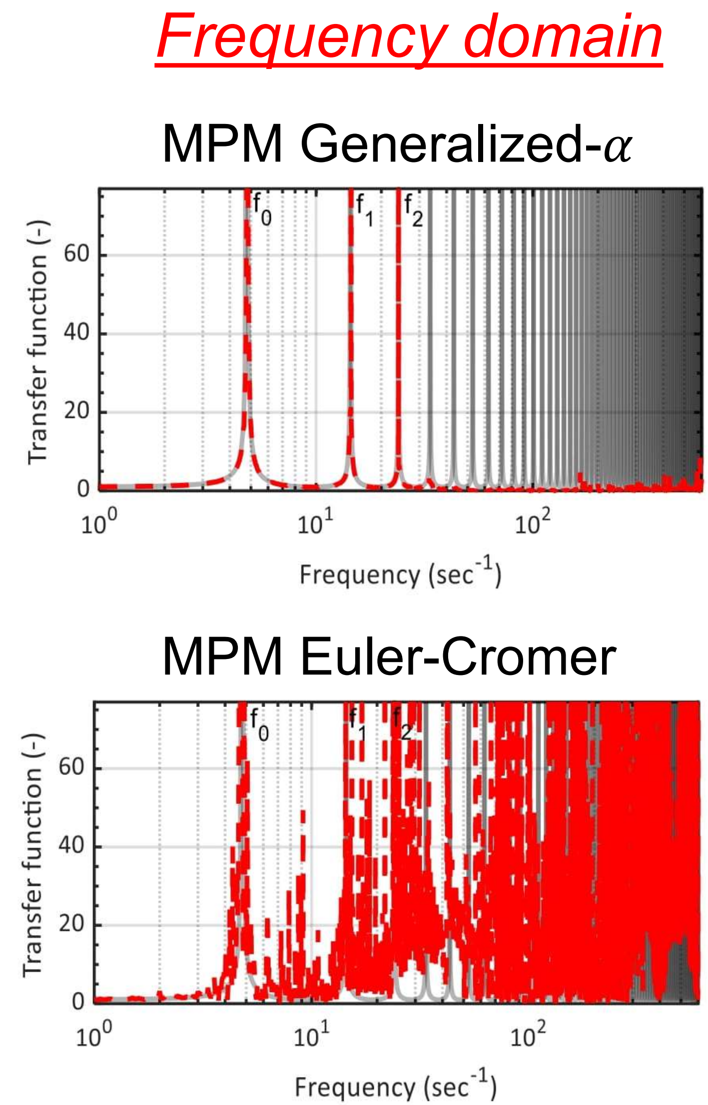

Large deformation with cell crossing

Alsardi & Yerro (2023)

Time domain

MPM Euler-Cromer | MPM Generalized-α

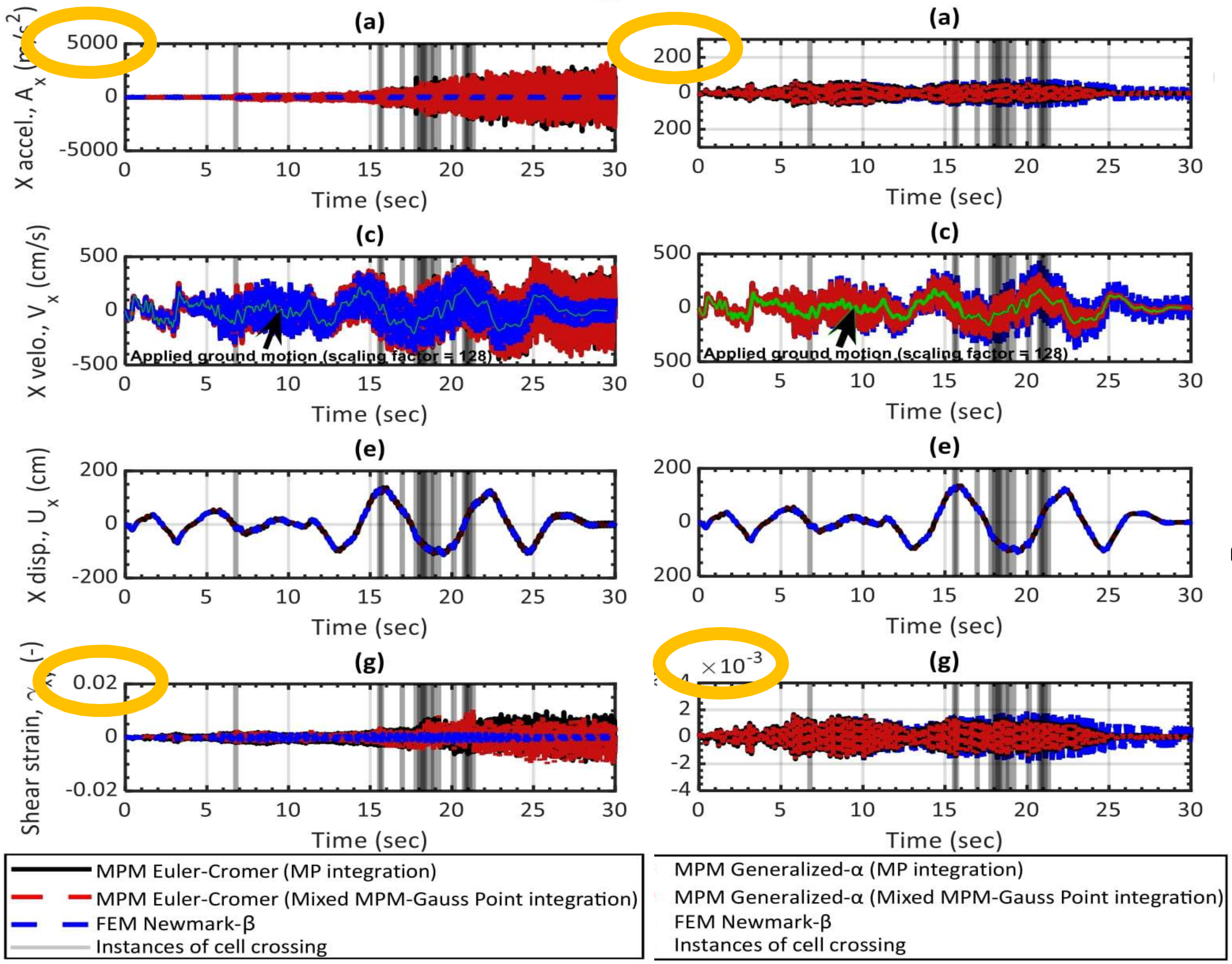

MP vs Gauss integration

Frequency domain

MPM Generalized-α

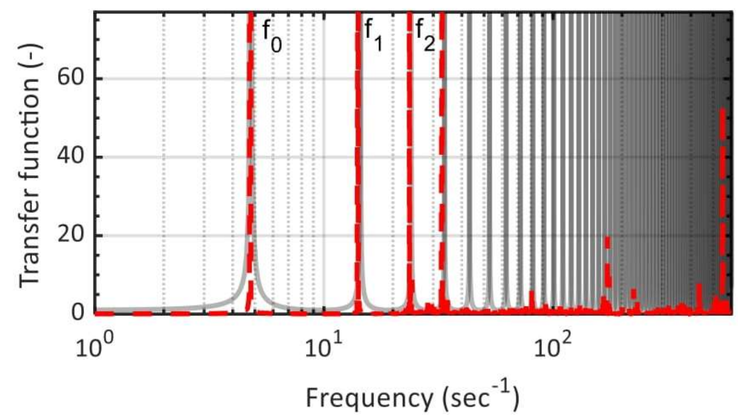

MPM Euler-Cromer

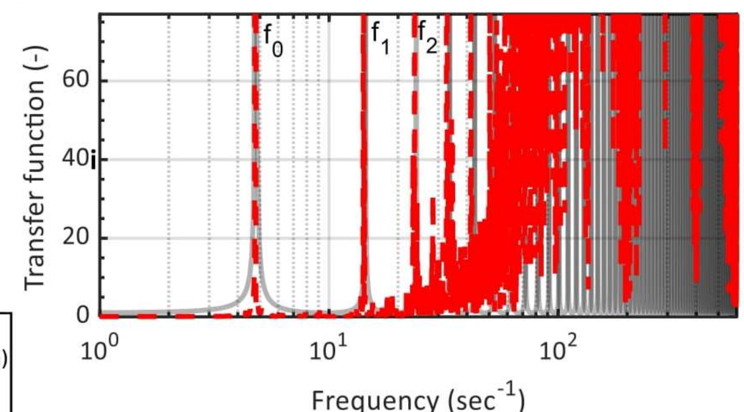

Parametric analysis of coseismic slope failures

Alsardi & Yerro (2023)

Effects of shaking intensity, embankment size, and material brittleness on runout

Small

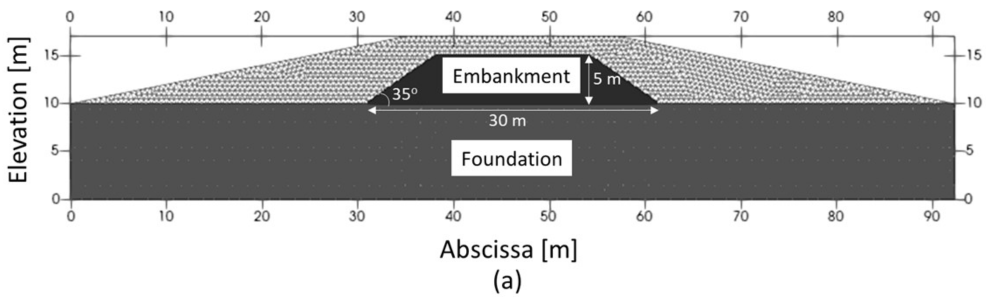

Large

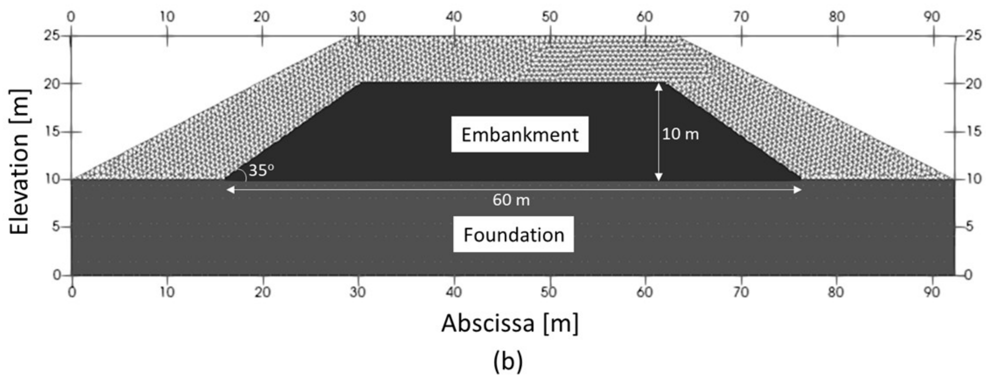

Material	Parameter	Value
Embankment (brittle)	Constitutive model	Mohr-Coulomb with strain-softening (MCSS)
	Peak friction angle, ϕ'_p (degrees)	37
	Residual friction angle, ϕ'_r (degrees)	20
	Peak cohesion, c'_p (kPa)	1
	Residual cohesion, c'_r (kPa)	0.5
	Exponential shape factor, η (-)	100
	Young's modulus, E (kPa)	10^6
	Poisson ratio, ν (-)	0.33
	Tension cutoff (kPa)	0
Embankment	Constitutive model	Mohr-Columb (MC)
	Friction angle, ϕ' (degrees)	37
	Cohesion, c' (kPa)	1
	Young's modulus, E (kPa)	10^6
	Poisson ratio, ν (-)	0.33
	Tension cutoff (kPa)	0
Foundation	Constitutive model	Linear-elastic
	Young's modulus, E (kPa)	10^6
	Poisson ratio, ν (-)	0.33

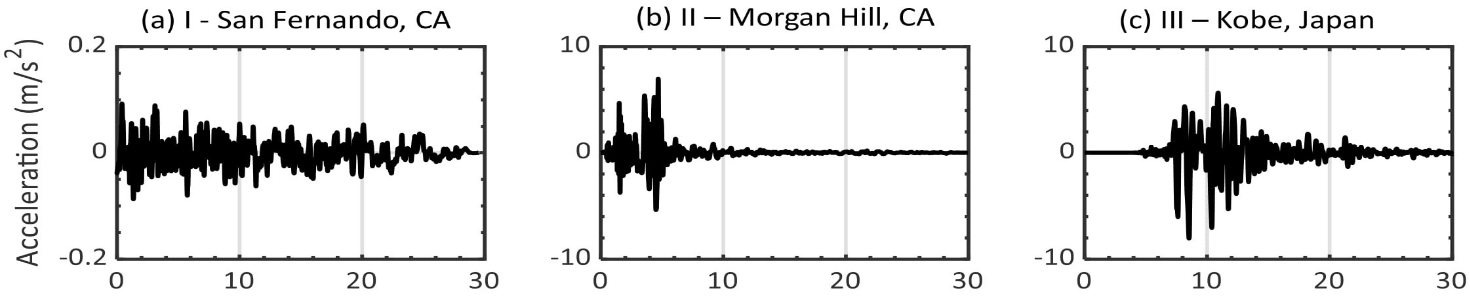

Parametric analysis of coseismic slope failures

Alsardi & Yerro (2023)

Effects of shaking intensity, embankment size, and material brittleness on runout

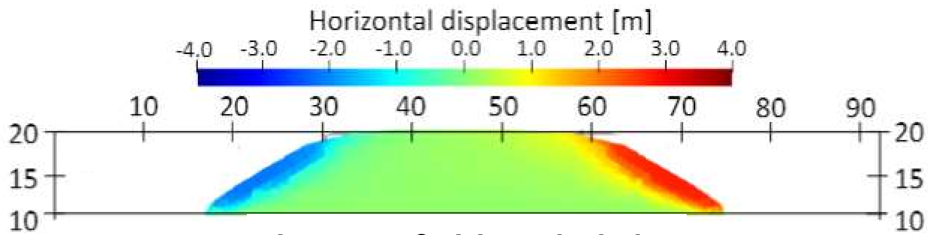

Large & Non-brittle

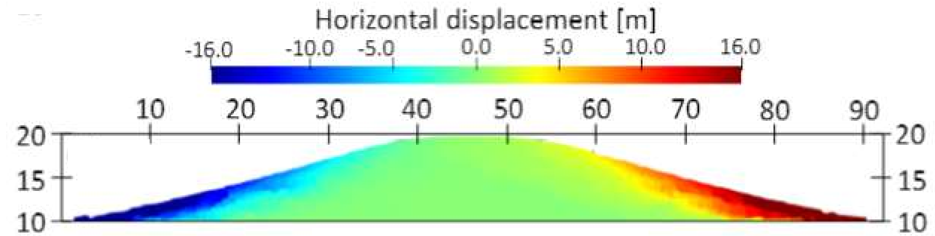

Large & Brittle

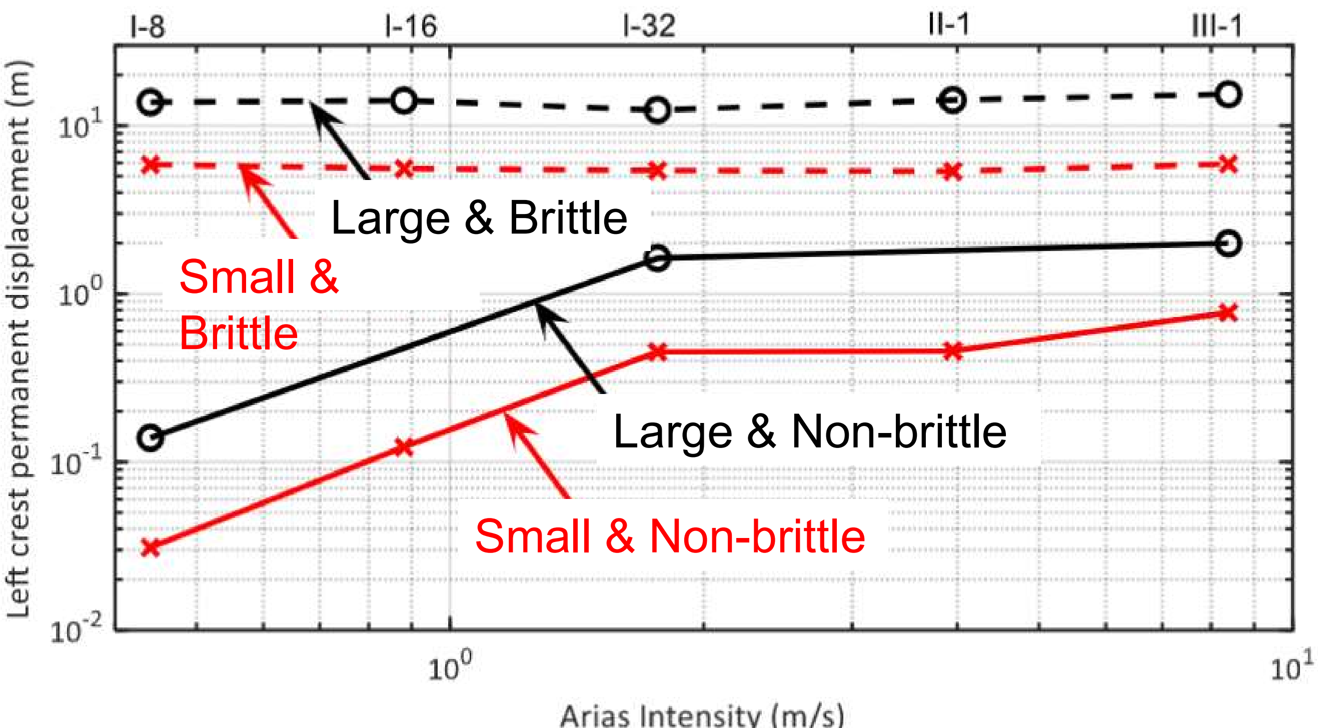

Alsardi, A. and Yerro, A. (2022) Coseismic site response and slope

Earthquake-triggered failures in saturated soils

Alsardi & Yerro (2024)

- Earthquake-induced liquefaction of earthen embankment
- Constitutive model: Intergranular Strain Anisotropy Hypoplastic Model

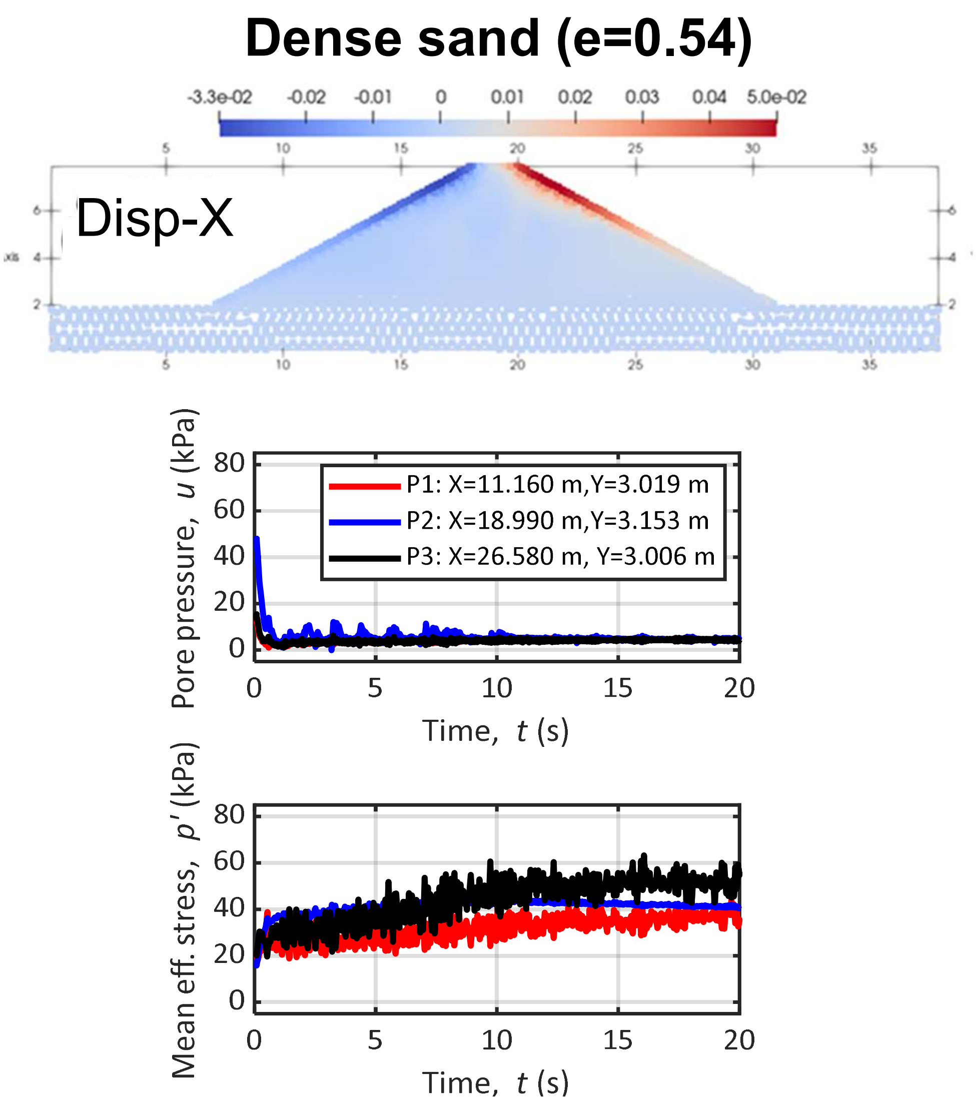

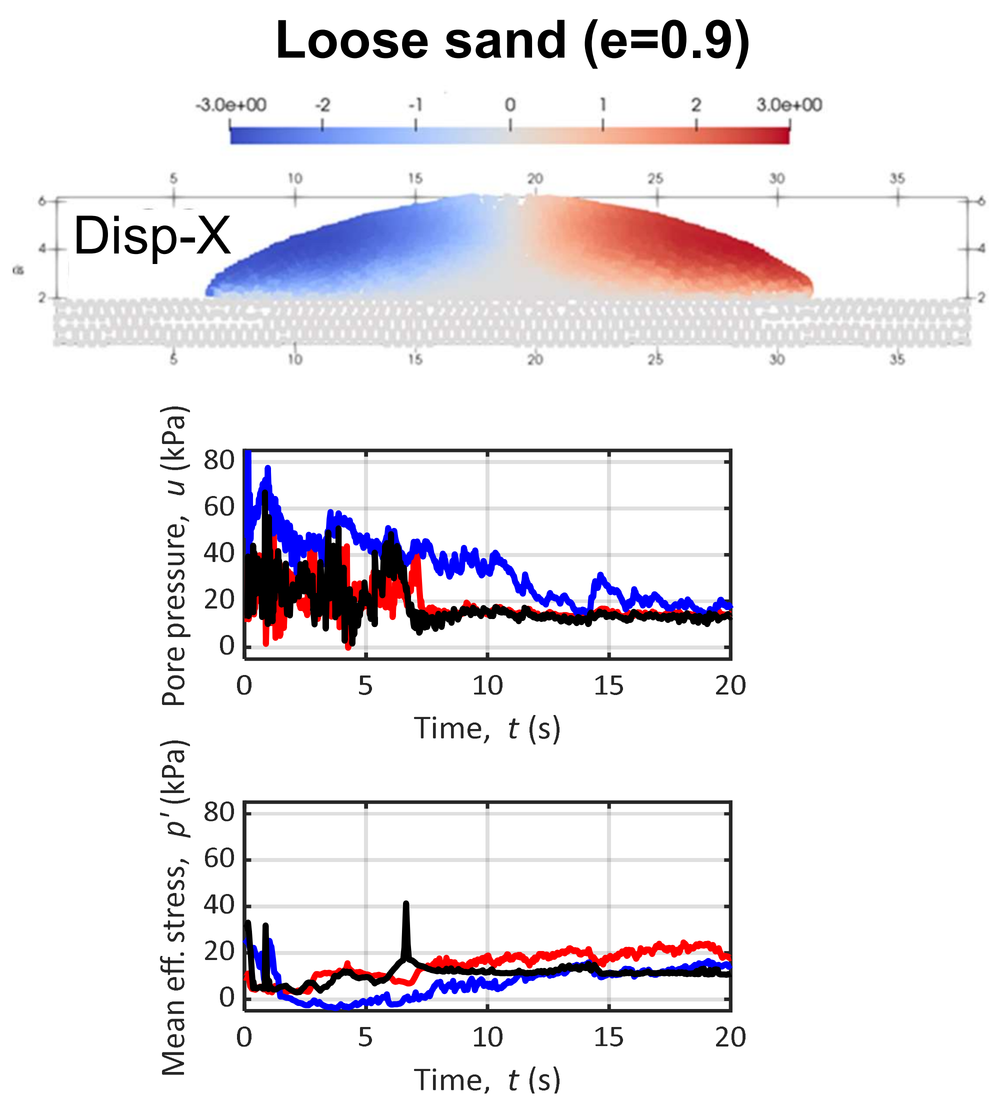

References

Alsardi, A., Copana, J., Yerro, A., 2021. *Modelling earthquake-triggered landslide run-out with the Material Point Method*. ICE Geotechnical Engineering, 174(5), 563-576.

Alsardi, A., Yerro, A., 2023. *Coseismic site response and slope instability using periodic boundary conditions in the material point method*. Journal of Rock Mechanics and Geotechnical Engineering, 15(3), 641-658.

Alsardi, A., Yerro, A., *MPM Coseismic Slope Runout Prediction Using the Intergranular Strain Anisotropy Hypoplastic Model*. Geo-Congress 2024, Vancouver, Canada, February 25-28, 2024.

Ceccato, F., Yerro, A., Girardi, V., Simonini, P., 2021. *Two-phase dynamic MPM formulation for unsaturated soil*. Computers and Geotechnics, 129, 103876.

Girardi, V., Yerro, A., Ceccato, F., Simonini, P., 2021. *Modeling large deformations in water retention structures with an unsaturated MPM approach*. ICE Geotechnical Engineering, 174(5), 577-592.

Murphy, J., Yerro, A., Soga, K., 2020*. A New Approach to Simulate Suffusion Processes with MPM.* In: Proc. Geo-Congress 2020. Minneapolis, U.S., February 2020.

Yerro, A., Alonso, E., Pinyol, N., 2015. *The material point method for unsaturated soils.* Géotechnique, 65(3), 201-217.

Yerro, A., Rohe, A., Soga, K., 2017. *Modelling internal erosion with the Material Point Method*. In: Proc. International Conference on the Material Point Method, Delft, The Netherlands.

Yerro, A., Girardi, V., Martinelli, M., Ceccato, F., 2022. *Modelling unsaturated soils with the Material Point Method.* A discussion of the state-of-the-art. Geomechanics for Energy and the Environment, 32, 100341.

Acknowledgements

Anura3D
MPM Research Community
www.anura3d.com

NSF Grant Numbers
CMMI-1937984
CMMI-2211002

GiD SIMULATION

Thanks for your attention

ayerro@vt.edu